

Geophysical Research Letters®



RESEARCH LETTER

10.1029/2025GL115265

Key Points:

- Fixed coordinate systems lead to significant smoothing in statistical studies of dynamic systems, such as the ionosphere
- Organizing ionospheric data relative to the poleward and equatorward boundaries of the auroral oval provides more representative statistical variations
- We use a new software package, OCBpy, to illustrate the impact of different adaptive co-ordinate systems on mean ionospheric vorticity

Correspondence to:

G. Chisham,
gchi@bas.ac.uk

Citation:

Chisham, G., Burrell, A. G., & Zawdie, K. A. (2025). The impact of adaptive high-latitude coordinates. *Geophysical Research Letters*, 52, e2025GL115265. <https://doi.org/10.1029/2025GL115265>




Received 7 FEB 2025

Accepted 1 AUG 2025

Author Contributions:

Conceptualization: Gareth Chisham, Angeline G. Burrell
Data curation: Gareth Chisham, Angeline G. Burrell
Formal analysis: Gareth Chisham, Angeline G. Burrell
Funding acquisition: Kate A. Zawdie
Investigation: Gareth Chisham, Angeline G. Burrell
Methodology: Gareth Chisham, Angeline G. Burrell
Software: Gareth Chisham, Angeline G. Burrell
Visualization: Gareth Chisham, Angeline G. Burrell
Writing – original draft: Gareth Chisham, Angeline G. Burrell
Writing – review & editing: Gareth Chisham, Angeline G. Burrell, Kate A. Zawdie

The Impact of Adaptive High-Latitude Coordinates

Gareth Chisham¹ , Angeline G. Burrell² , and Kate A. Zawdie² 

¹British Antarctic Survey, Cambridge, UK, ²Space Science Division, U.S. Naval Research Laboratory, Washington, DC, USA

Abstract The high-latitude ionosphere can be divided into three regions dominated by different types of coupling and characterized by distinctive behaviors. These are the polar cap, the auroral region, and the sub-auroral region. Their locations are highly variable, changing in extent in response to driving conditions in the solar wind and within the magnetosphere. We discuss how defining high-latitude coordinates relative to the boundaries between these physically significant regions (adaptive co-ordinates) has major implications for statistical studies, modeling applications, and research combining magnetospheric and ionospheric data. We explore the impact of using adaptive co-ordinates for statistical analyses of ionospheric vorticity, showing how using adaptive co-ordinate systems provides a clearer picture of the latitudinal variation of vorticity, and how peaks and troughs in vorticity relate to the boundary locations.

Plain Language Summary The high-latitude ionosphere, which covers the Arctic and Antarctic regions at altitudes of between 80 and 600 km, is a complex region which is affected by energy from the solar wind that flows out from the sun, and strongly couples with other components of the near-Earth space environment (the magnetosphere and neutral atmosphere). One way to visualize the ionosphere at high latitudes is to consider which portions of the magnetosphere and ionosphere are connected. This creates three different regions with distinctive characteristics: the polar cap, the auroral region, and the sub-auroral region, whose locations relative to the surface of the Earth change in response to changes in the solar wind input. It is important to define high-latitude coordinates relative to the boundaries between these physically significant regions, especially when looking at data sets gathered over long time periods, or when attempting to model processes. This study explores the impact of using single or multiple boundaries for such high-latitude research efforts.

1. Introduction

Coupling within the Atmosphere-Ionosphere-Magnetosphere (AIM) system and the solar wind is most entwined in the high latitude ionosphere, which covers the Arctic and Antarctic regions. Here, it is possible to identify three distinct ionospheric regions (the polar cap, the auroral region, and the sub-auroral region), based on the area of the magnetosphere to which they are connected.

The most poleward region, the polar cap, is the area characterized by open magnetic field lines that connect directly to the interplanetary magnetic field (IMF) instead of closing in the opposite hemisphere. Within the polar cap, ionospheric plasma typically moves anti-sunward (Dungey, 1961), though it will deviate from this path due to the angle at which the IMF and the magnetosphere connect (Cowley & Lockwood, 1992). Precipitation in the polar cap is typically characterized by weak, low-energy electron precipitation (Sotirelis & Newell, 2000). However, it is also home to distinct but transient ionospheric structures, such as polar patches (Eriksen et al., 2023) and polar arcs (Reidy et al., 2018).

Immediately equatorward of the polar cap is the auroral region, which experiences large amounts of particle precipitation and significant energy transfer between the magnetosphere and ionosphere along closed magnetic field lines. Within the auroral region, ionospheric plasma moves sunward, completing the Dungey cycle (Cowley & Lockwood, 1992; Dungey, 1961). The auroral region is characterized by a wealth of large structures, such as auroral arcs (Karlsson et al., 2020), and smaller structures, such as filaments, curls, and pulsating aurora (Davis, 1978; Kataoka et al., 2021). The poleward and equatorward boundaries of the auroral region mark the approximate locations of the peak Region 1 and Region 2 Field-Aligned Currents (FAC), respectively, that flow between the ionosphere and magnetosphere, and close predominantly across the auroral region (Iijima & Potemra, 1976).

© 2025. The Author(s).

This is an open access article under the terms of the [Creative Commons Attribution License](https://creativecommons.org/licenses/by/4.0/), which permits use, distribution and reproduction in any medium, provided the original work is properly cited.

The equatorward edge of the auroral region marks the transition to the sub-auroral region. Although the sub-auroral region is typically equatorward of the strongest sunward convection flows, phenomena such as Strong Thermal Emission Velocity Enhancement (STEVE) (MacDonald et al., 2018) and Sub-Auroral Polarization Streams (SAPS) (Foster & Burke, 2002) are observed during geomagnetically disturbed intervals. Large-scale Traveling Ionospheric Disturbances (LSTIDs) and Traveling Atmospheric Disturbances (TADs) are also observed to travel equatorward from this boundary (Lyons et al., 2019).

Defining high latitude coordinate systems relative to the physically significant boundaries between these distinct regions can have major implications for statistical studies of these regions and associated phenomena, for modeling applications, and for research that involves the combination of different AIM data sets. Figure 1 explains this impact schematically. Panel (a) shows example observations of a heightened intensity feature that is contained within two physical boundaries, the locations of which vary in response to changes in the driving of the system (e.g., magnetic flux being added or removed from the polar cap through magnetic reconnection). Panel (b) presents a schematic that describes the statistical intensity variation if these intensity features are averaged together in a fixed co-ordinate system. The shaded regions show that statistical variations at the edges of this averaged intensity feature bear no resemblance to the true intensity variations at the boundary. Panel (c) presents a schematic that describes the statistical intensity variation in adaptive co-ordinates, where the intensity measurements are binned and averaged at locations relative to identified physical boundaries such as the Open-Closed magnetic field line Boundary (OCB) and the Equatorward Auroral Boundary (EAB). Hence, the latitude grid in adaptive co-ordinates is defined by position relative to variable boundary locations (Chisham, 2017).

Although there have been occasional analyses of this type, adaptive co-ordinate gridding is not in common usage, often because of the lack of available boundary data, or of the software required for the analyses. To address this we have developed OCBpy, a free and open source software project designed to convert between geographic, geodetic, or magnetic coordinates and boundary-oriented adaptive coordinates (Burrell et al., 2025). In this study, we demonstrate how OCBpy can be used in combination with publicly available estimations of the OCB and EAB derived from Imager for Magnetosphere-to-Aurora Global Exploration (IMAGE) Far Ultraviolet (FUV) observations (Chisham, 2022; Chisham et al., 2022) to examine the impact of using different coordinate systems on the statistical analysis of high-latitude ionospheric observations. We compare results from using the Altitude Adjusted Corrected GeoMagnetic (AACGM-V2) coordinate system (Shepherd, 2014), adaptive coordinates considering a single boundary (both the OCB and EAB individually), and adaptive coordinates that consider both the OCB and EAB (dual boundary).

Section 2 provides an overview of the boundaries used in this study and the ionospheric data set that will be used to assess the impact of the different coordinate systems. Section 3 presents the analysis methodology. Section 4 presents the statistical studies for the different coordinate systems. Section 5 discusses the methods, the study and plans for future research.

2. Data

Two types of data are used in this paper: the high latitude boundary data (from IMAGE FUV), described in Section 2.1, and the ionospheric data (SuperDARN vorticity), described in Section 2.2.

2.1. IMAGE FUV Boundaries

The FUV detectors aboard the IMAGE spacecraft (Burch, 2000; Mende et al., 2000a, 2000b), namely the Wideband Imaging Camera (WIC) (Mende et al., 2000a, 2000b, 2000c), and the two Spectrographic Imagers (SI12 and SI13) (Mende et al., 2000c), provided full or partial images of the northern hemisphere auroral region at three different wavelengths from 5 May 2000 to 30 September 2002. The boundaries used in this study were estimated from the FUV images (Boakes et al., 2008; Chisham et al., 2022; Longden et al., 2010), and adjusted to correspond to the OCB and EAB using calibrations determined by statistical comparison with the Defense Meteorological Satellite Program (DMSP) Particle Precipitation Boundaries (PPBs) (Chisham, 2022; Chisham et al., 2022). The PPBs, determined from high-resolution in situ DMSP Special Sensor J/4 (SSJ/4) precipitating electron and ion measurements (Newell et al., 1991, 1996; Sotirelis & Newell, 2000), represent the most precise and accurate boundary estimates. However, the DMSP PPBs do not provide sufficient spatial and temporal coverage to define the boundary variations across all longitudes. Hence, we use the statistically corrected FUV boundaries to provide OCB and EAB proxies at all MLTs at a cadence as low as 2 min. The daily availability of

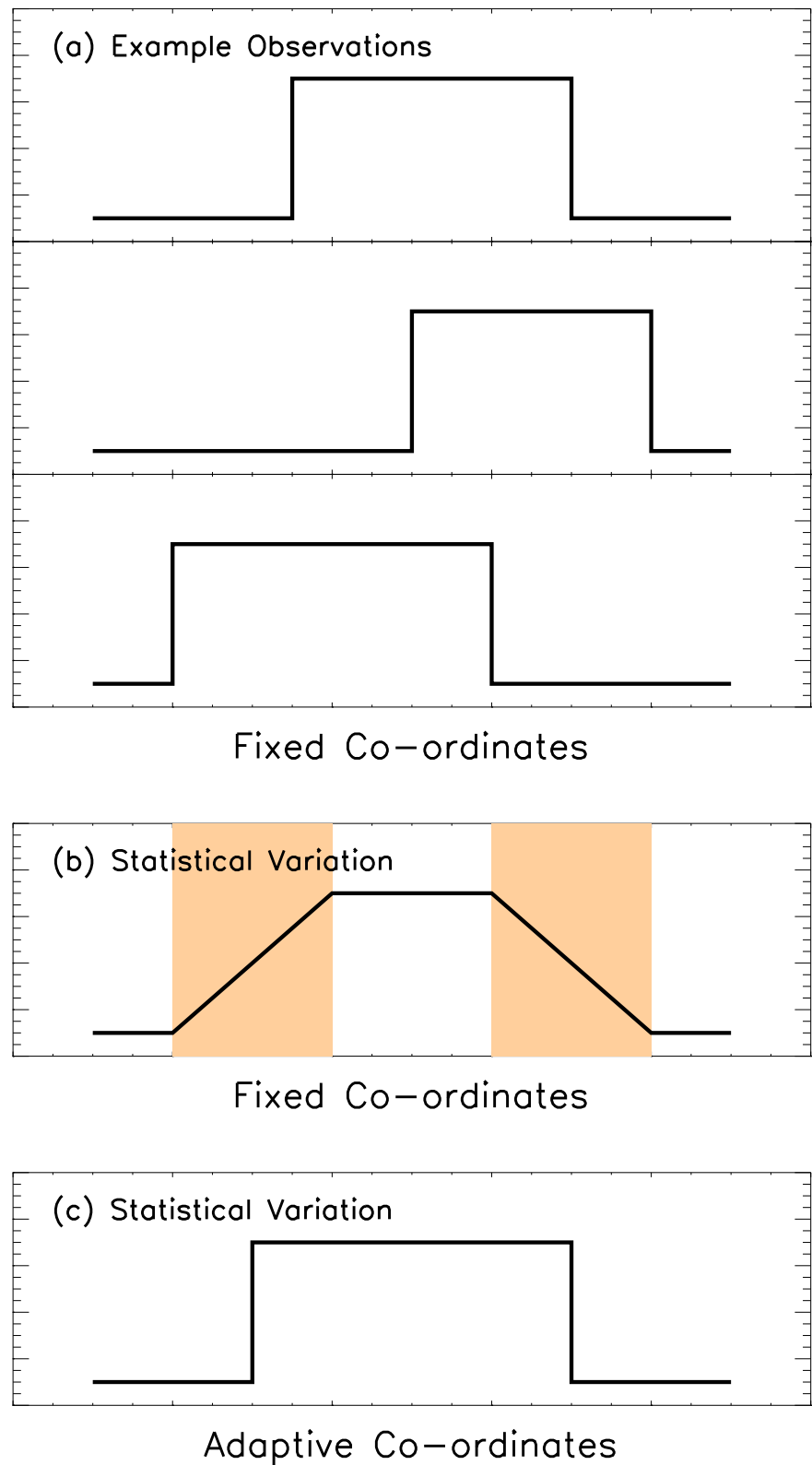


Figure 1. Schematic representation of the impact of gridding measurements of moving physical structures in fixed and adaptive co-ordinate systems. (a) Example observations in fixed co-ordinates; (b) A statistical representation of the structure in fixed co-ordinates; (c) A statistical representation of the structure in adaptive co-ordinates.

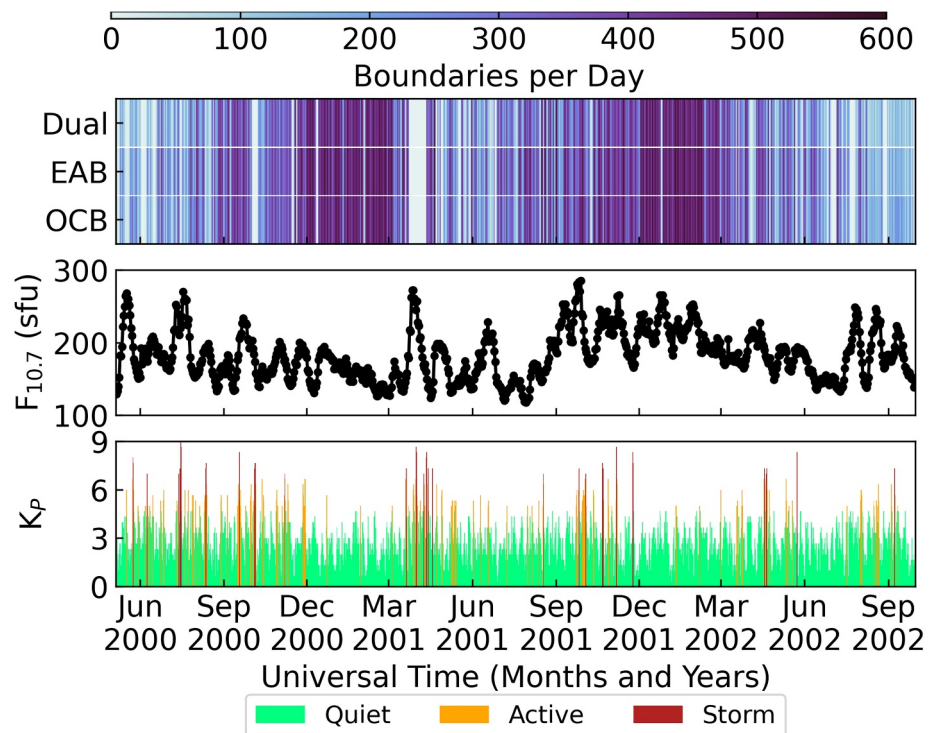


Figure 2. (a) Temporal variation of the number of IMAGE FUV boundaries (OCB, EAB, and Dual) observed per day across the measurement epoch (May 2000 to October 2002). (b) The $F_{10.7}$ index variation across the measurement epoch. (c) The K_p index variation across the measurement epoch.

these OCB and EAB proxies is shown in Figure 2, which also presents solar ($F_{10.7}$) and geomagnetic (K_p) indices as a function of Universal Time (UT) over the period of IMAGE boundary availability, for context.

2.2. SuperDARN Vorticity

The Super Dual Auroral Radar Network (SuperDARN) is an international network of high frequency (HF) coherent scatter radars with fields of view (FOV) that cover the mid- and high-latitudes in both the northern and southern hemispheres (Chisham et al., 2007; Greenwald et al., 1995; Nishitani et al., 2019). These radars measure the line-of-sight (LOS) Doppler velocity of ionospheric irregularities in the F-region ionosphere that move with the background ionospheric plasma flow. When radar FOV overlap, it is possible to construct two-dimensional vectors of the ionospheric flow velocity (Hanuise et al., 1993) and further examine changes in adjacent observations to measure the local flow vorticity (Chisham et al., 2009; Chisham & Freeman, 2023). Vorticity can be used to study the motion of both large-scale and meso-scale structure in the F-region ionosphere (Chisham & Freeman, 2024). The vorticity data set used in this study (Chisham, 2023) covers the interval 2000–2005 inclusive, and uses observations from three SuperDARN radar pairs covering the AACGM latitude range 66° to 86° : Goose Bay (GBR) and Stokkseyri (STO), Prince George (PGR) and Kodiak (KOD), and Kapuskasing (KAP) and Saskatoon (SAS). In this data set, a positive vorticity relates to a clockwise rotation when looking in the direction of the magnetic field into the northern hemisphere ionosphere, and a negative vorticity relates to an anti-clockwise rotation.

3. Methodology

The pairing of the ionospheric vorticity measurements with the IMAGE FUV boundaries was performed using OCBpy v0.5.0 (Burrell et al., 2025). Every pair of measurements are required to be contemporaneous and co-located in MLT sector. The vorticity data are initially gridded in AACGM-V2 coordinates, and then regridded in adaptive coordinates considering first, single boundaries (the OCB and EAB individually), and second, both the OCB and EAB together (dual boundary). If a vorticity measurement is located between two boundaries it is

gridded by its latitudinal position in relation to both these boundaries. If a measurement is located either below or above both boundaries, or only a single boundary is being considered, it is gridded solely by its latitudinal location in relation to the nearest boundary. Hence, in the dual boundary case the scaling of the latitude grid is different depending on whether the measurement is between or outside of the two boundaries. In addition to this regridding, the SuperDARN vorticities were scaled as described in Chisham (2017) to ensure appropriate magnitudes of electromagnetic properties across the polar cap. This scaling is also available within OCBpy.

Figures 3a, 3c, 3e, and 3g show the spatial variation of the mean SuperDARN vorticity values measured between the start of 1 January 2000 and the end of 31 December 2002, when represented in all these co-ordinate systems. The means were calculated using bins of 1° latitude and 1 hr of magnetic local time (MLT), and at least 100 values are required in a bin for an acceptable mean estimation. In AACGM-V2 co-ordinates a 1° latitude bin is clearly defined. In the adaptive co-ordinate systems there is no “pre-defined latitude” value for any measurement and hence, a bin does not have a fixed latitudinal value. Each measurement is characterized by a latitudinal difference in relation to the observed boundaries (as discussed above), and hence the bins used in the regridding are all ordered by these latitudinal differences. Hence, for visualization of the means of the regridded data in adaptive co-ordinates we need to set the boundaries at fixed latitudinal locations. Here, we choose 74° for the OCB and 64° for the EAB, which are close to the average locations of these boundaries in our boundary database. The limited availability of the IMAGE FUV boundaries reduces the number of observations that can be used to calculate the means in the adaptive coordinates. The number of points available to calculate the mean in each latitude-local time bin (Figures 3b, 3d, 3f, and 3h) highlights the variability of the auroral oval: despite the latitude limitations in AACGM-V2 coordinates, the radars observe enough sub-auroral and polar cap data across all local times to obtain meaningful averages in the inner portion of the polar cap and the high-latitude portion of the sub-auroral zone.

4. Results

Figure 3a presents the spatial variation of the mean vorticity in AACGM-V2 co-ordinates, similar to the representation of the same data in Chisham et al. (2009); the minimum latitude of the observations is limited to 66° in this co-ordinate system due to the physical location of the minimum latitude of the radar FOVs. The variation shows clearly defined regions associated with the co-located field-aligned current systems: Region 2 (equatorward of 70°), Region 1 (between 70° and 80°), and northward B_z (NBZ—poleward of 80° on the dayside).

Figure 3c presents the variation in adaptive co-ordinates when only the location of the OCB is considered. Here, Region 1 and Region 2 are again clear, but the intensities in the NBZ system are reduced. This is most likely due to the OCB being poorly defined during intervals of northward IMF. Future work separating this analysis by IMF direction would clarify this. The latitudinal width of Region 1 is reduced; the OCB is shown to be positioned close to the peak in the mean intensity in this region. The use of this co-ordinate system also shows that SuperDARN measures Region 2 vorticities for an extended region equatorward of the OCB location and the peak Region 1 vorticity (up to $\sim 14^\circ$ equatorward). However, the magnitude of the Region 2 mean vorticity values appears reduced and the peak is not well defined.

Figure 3e presents the variation in adaptive co-ordinates when only the location of the EAB is considered. This method of adaptive gridding presents results most similar to that in AACGM-V2 magnetic coordinates due to the locations of the data used in this study. The same regions exist, but differ in extent in different MLT sectors. On the duskside the latitudinal width of Region 1 is increased, whereas the latitudinal width of Region 2 is reduced. The statistical EAB location appears to be located a few degrees equatorward of the transition between Region 1 and Region 2 (zero vorticity).

Figure 3g presents the variation in adaptive co-ordinates when both the OCB and the EAB locations are considered (dual boundary). The mean vorticity variations across all regions are now the most distinct. The variation poleward of the OCB is similar to that seen in Figure 3c, whereas that equatorward of the EAB best matches that in Figure 3e. The Region 1 to Region 2 transition between these boundaries is now clearly defined. It is not possible to derive this relationship to these physical boundaries from the representations in any of the previous co-ordinate systems.

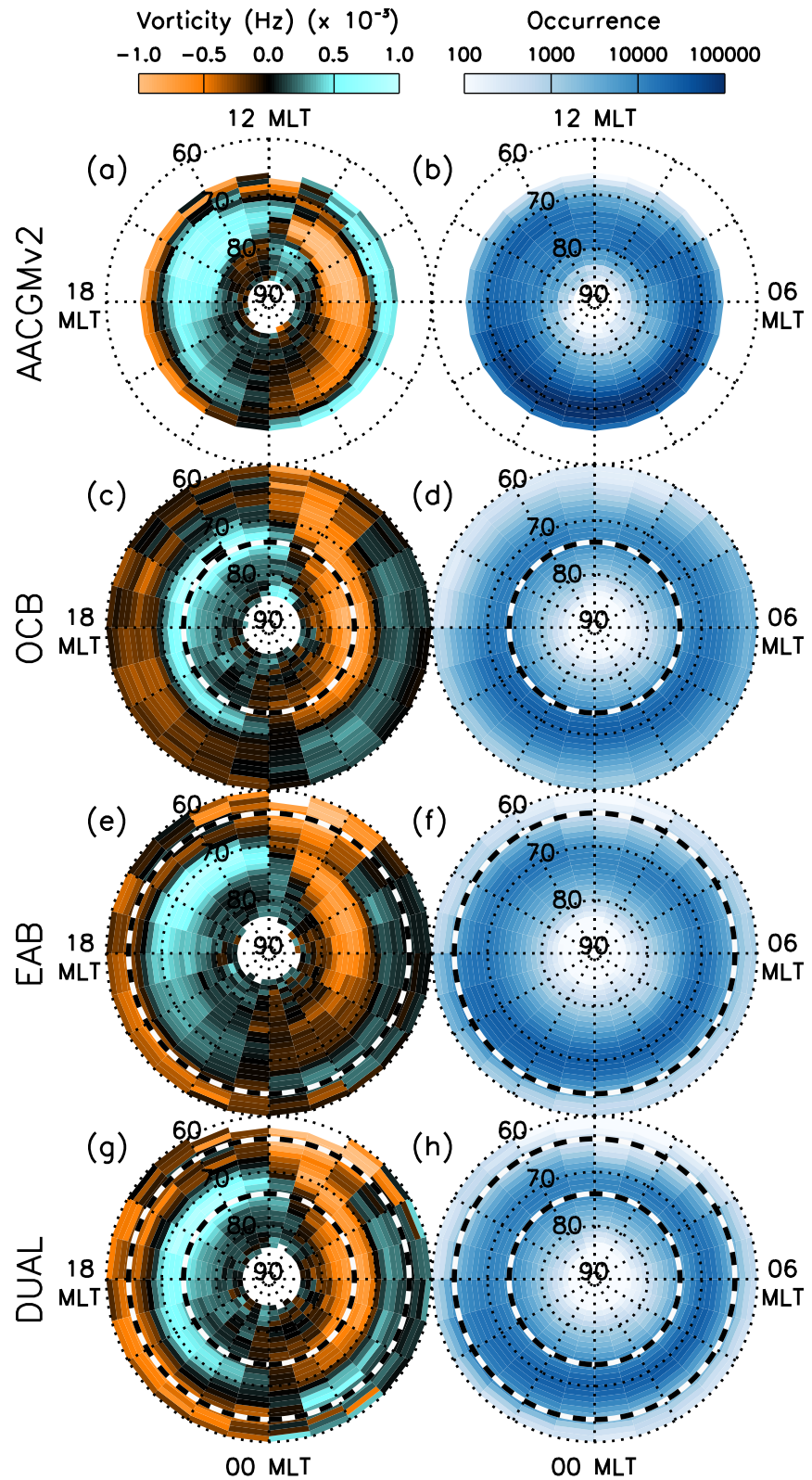


Figure 3. The SuperDARN mean vorticity as a function of magnetic or adapted latitude and local time (left column) and the number of points used to calculate each mean (right column) in AACGMV2 (a, b), OCB (c, d), EAB (e, f), and dual (g, h) co-ordinates. The black and white dashed circles represent the locations of the boundaries for the adaptive co-ordinate systems.

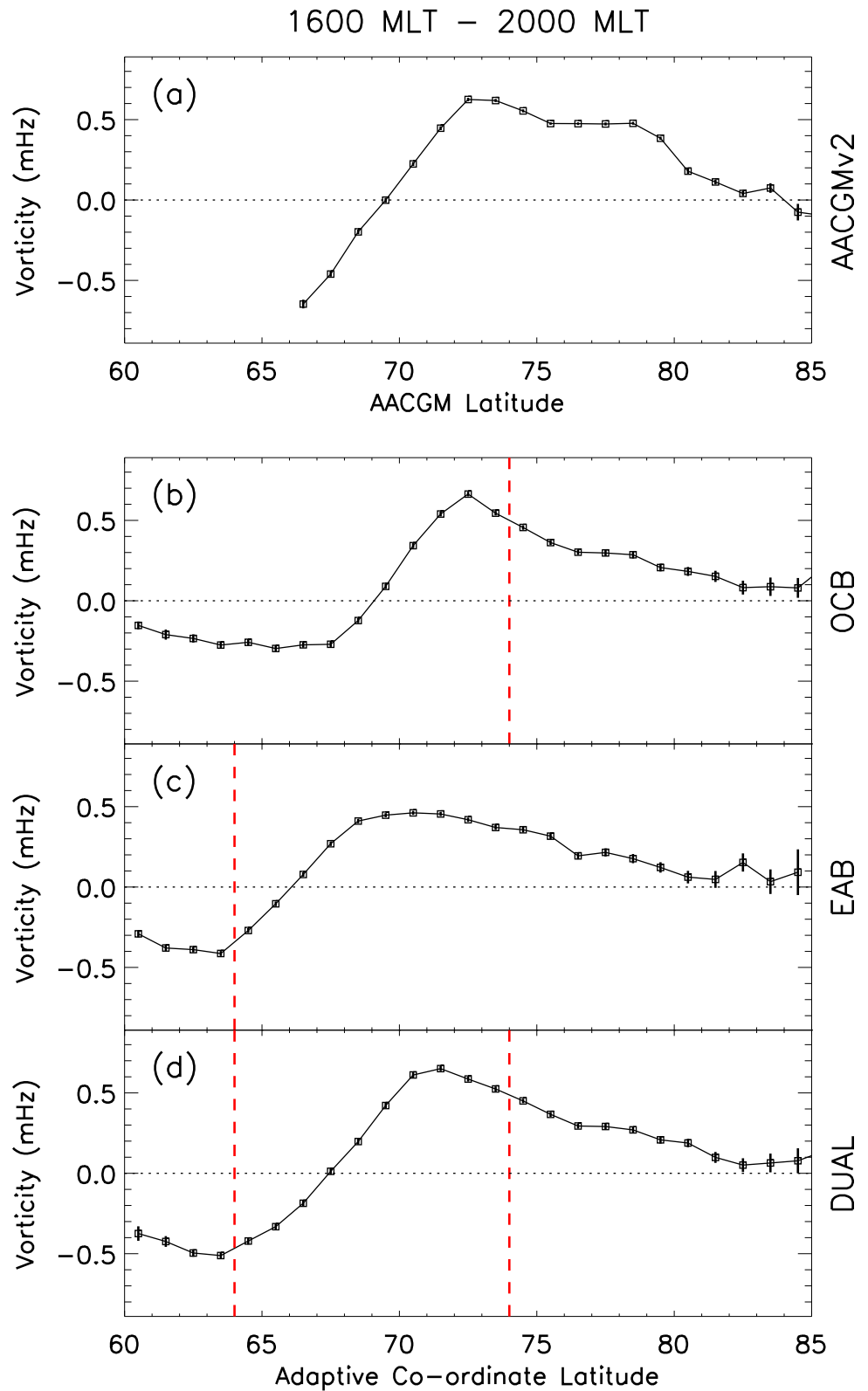


Figure 4. The latitudinal variation of the mean (and error on the mean) of vorticity measured between 16:00–20:00 MLT for (a) AACGM-V2, (b) OCB, (c) EAB, and (d) dual co-ordinate systems. The red vertical dashed lines represent the locations of the boundaries in the adaptive co-ordinate systems.

To show this increased clarity in the spatial variation of the mean vorticity with respect to the boundaries, we show in Figure 4 the mean vorticity as a function of latitude when considering all measurements between 16:00 and 20:00 MLT.

Figure 4a presents the latitudinal variation of mean vorticity when gridded in AACGM-V2 co-ordinates. Here, the latitudinal variation is limited at the lowest latitudes by the low-latitude limit of the radar FOVs. Even though the data have not been gridded in relation to any boundaries, and hence the measurements from different physical regions have been averaged together, there is still a very clear variation from negative mean vorticity at lower latitudes (Region 2) to positive mean vorticity at higher latitudes (Region 1), tapering to approximately zero mean vorticity at the highest latitudes (in the polar cap).

The change to adaptive co-ordinates (relative to the OCB) in Figure 4b shows three things clearly that were hinted at in the contour plots in Figure 3: (a) there are measurements far equatorward of the OCB that are not easily identified as such when using fixed AACGM co-ordinates; (b) the Region 1 peak mean vorticity is located slightly equatorward of the OCB, and not co-incident with it; and (c) the latitudinal variation of the mean vorticity is more clearly defined around the OCB location. Similarly, the change to adaptive co-ordinates relative to the EAB in Figure 4c results in more clearly defined variations about the EAB location, highlighting that the largest negative mean vorticity occurs at the EAB. This suggests that the EAB is co-located with the Region 2 peak. Using adaptive co-ordinates considering both the OCB and EAB (dual) results in a more clearly defined latitudinal variation, as presented in Figure 4d, highlighting the relationship of the peak mean vorticity in both Regions 1 and 2, and the transition between these two regions, with both boundaries.

5. Discussion

The analysis in this paper clearly shows the effect that the choice of co-ordinate system has on the statistical representation of ionospheric measurements. The standard method of presenting statistical information, in fixed co-ordinate systems, is flawed due to the dynamical nature of the magnetosphere-ionosphere system. In our example, we do not see the full extent of how much of the Region 2 system has been measured. Many of the Region 2 vorticity measurements are being averaged together with the Region 1 vorticity data. This failure of using fixed co-ordinates becomes clear when using adaptive co-ordinates. Second, it is clear that the latitudinal extent of the Region 1 system is overestimated when using fixed co-ordinates due to the smoothing that is a consequence of not considering the dynamics of the boundaries.

Our analysis presents three examples of adaptive high-latitude coordinate systems that organize data based on their relationship to important high-latitude physical boundaries (the OCB and EAB). Although all three examples improve the representation of the data, the dual boundary methodology provides the most significant advantages. Here, there is a very clear structure in the latitudinal variation of the vorticity—how the vorticity peaks and troughs relate to the two boundaries is now very clearly defined. Of particular interest is the fact that the Region 1 peak mean vorticity is located equatorward of the OCB, which can not be determined from the variation in fixed co-ordinates. These new insights from using adaptive co-ordinates will lead to vastly improved modeling of processes in these regions.

There have also been other studies that have considered the use of adaptive co-ordinate systems. Redmon et al. (2010) and Chisham (2017) demonstrated the importance of using OCB coordinates in statistical studies, showing that polar and auroral signatures would be averaged together if magnetic coordinates were used instead. Zhu et al. (2019) demonstrated that scaling high-latitude model inputs relative to the Convection Reversal Boundary (CRB), a boundary defined by the shear in the ionospheric convection flow that is related to the OCB, resulted in more realistic Joule heating within a first principles model. The improved Joule heating specification then impacted the global electrodynamics within the model. Reistad et al. (2021) used OCB coordinates to examine the impact of lobe reconnection rates on flux transport, finding that during times when the IMF B_y component is dominant, lobe reconnection can account for a significant portion of the Dungey cycle flux transport (with this portion being larger in the summer hemisphere). Landry and Anderson (2018) created an empirical model of SAPS electric fields, using particle precipitation measurements to determine whether observations were made at sub-auroral latitudes or not. Their SAPS model presented results in degrees of magnetic latitude equatorward of the EAB, allowing easy conversion of the model to standard magnetic or geodetic coordinates. Sotirelis and Newell (2000) developed an adaptive co-ordinate model of DMSF particle precipitation by binning data in dynamic boundary-oriented co-ordinates, based on the multiple regions and boundaries defined by Newell

et al. (1991, 1996). More recently, Wu et al. (2021) developed an auroral model using Polar Ultraviolet Imager data that combined auroral intensity data based on the cumulative energy between the poleward and equatorward auroral luminosity boundaries. They found that developing the model in this way preserved the peak intensity of the energy flux, which resulted in a better comparison with DMSP SSUSI data than the Ovation Prime model (Newell et al., 2014).

This work shows that gridding measurements relative to physical boundaries is essential when developing climatological models, examining statistical behavior, or placing magnetospheric boundaries in first-principles models, since these boundaries have variable locations in fixed co-ordinate systems. Ignoring the movement of these boundaries results in over-smoothing of features that are present near transition regions (see Figure 1). Using coordinate systems constrained by physical boundaries provides greater scientific insight.

The major issue with adaptive co-ordinate analysis is that simultaneous measurements of boundaries at sufficient local times to provide a complete specification are difficult to obtain. This lack of observations needs to be remedied in the future, through an investment in ground- and space-based auroral imagers in both the northern and southern hemispheres, as well as particle precipitation detectors in low Earth orbit. When such observations are available, it is possible to undertake the type of statistical examination of data that has been presented here. In the event that only one of the desired boundaries is well specified, improvements can still be made in the interpretation of measurements near that boundary. Indeed, for certain scientific questions it may only be necessary to account for the location of either the OCB or EAB, and not both.

Plans for future improvements to these coordinate systems include expanding the available database of boundary observations in OCBpy and allowing the use of boundaries provided by empirical models as well as observations. This future work includes the creation of one such empirical model. This is expected to positively impact space weather modeling, as it allows improved specification of various magnetospheric inputs that include Joule heating and energetic particle precipitation.

Data Availability Statement

The SuperDARN vorticity data used in this paper are available through Chisham (2023), <https://doi.org/10.5285/8EEDC594-730B-4AAD-B9CE-827912320C3A>. The raw SuperDARN data are available through the BAS SuperDARN data mirror (<https://www.bas.ac.uk/project/superdarn/>). The IMAGE FUV boundary data used here can be found at <https://doi.org/10.5285/fa592594-93e0-4ee1-8268-b031ce21c3ca> (Chisham, 2022). The raw image data, and software, were acquired from <http://sprg.ssl.berkeley.edu/image/>. The fitted circle boundaries are available within OCBpy (Burrell et al., 2025).

References

- Boakes, P. D., Milan, S. E., Abel, G. A., Freeman, M. P., Chisham, G., Hubert, B., & Sotirelis, T. (2008). On the use of IMAGE FUV for estimating the latitude of the open/closed magnetic field line boundary in the ionosphere. *Annales Geophysicae*, 26(9), 2759–2769. <https://doi.org/10.5194/angeo-26-2759-2008>
- Burch, J. L. (2000). Image mission overview. In J. L. Burch (Ed.), *The Image Mission* (pp. 1–14). Springer. https://doi.org/10.1007/978-94-011-4233-5_1
- Burrell, A. G., Chisham, G., & Reistad, J. (2025). *aburrell/ocbpy: v0.5.0*. Zenodo. <https://doi.org/10.5281/zenodo.14756066>
- Chisham, G. (2022). Ionospheric boundaries derived from IMAGE satellite mission data (May 2000–October 2002), version 2.0 [Dataset]. *NERC EDS UK Polar Data Centre*. <https://doi.org/10.5285/fa592594-93e0-4ee1-8268-b031ce21c3ca>
- Chisham, G. (2017). A new methodology for the development of high-latitude ionospheric climatologies and empirical models. *Journal of Geophysical Research*, 122(A1), 932–947. <https://doi.org/10.1002/2016JA023235>
- Chisham, G. (2023). Ionospheric vorticity across the northern hemisphere ionosphere determined from particular SuperDARN radar pairs—2000 to 2005 inclusive (version 1.0) [Dataset]. *NERC EDS UK Polar Data Centre*. <https://doi.org/10.5285/8eedc594-730b-4aad-b9ce-827912320c3a>
- Chisham, G., Burrell, A. G., Thomas, E. G., & Chen, Y.-J. (2022). Ionospheric boundaries derived from auroral images. *Journal of Geophysical Research*, 127(A7), e2022JA030622. <https://doi.org/10.1029/2022JA030622>
- Chisham, G., & Freeman, M. P. (2024). The spatial variation of large- and meso-scale plasma flow vorticity statistics in the high-latitude ionosphere and implications for ionospheric plasma flow models. *Journal of Geophysical Research*, 129(A7), e2024JA032887. <https://doi.org/10.1029/2024JA032887>
- Chisham, G., & Freeman, M. P. (2023). Separating contributions to plasma vorticity in the high-latitude ionosphere from large-scale convection and meso-scale turbulence. *Journal of Geophysical Research*, 128(A9), e2023JA031885. <https://doi.org/10.1029/2023JA031885>
- Chisham, G., Freeman, M. P., Abel, G. A., Bristow, W. A., Marchaudon, A., Ruohoniemi, J. M., & Sofko, G. J. (2009). Spatial distribution of average vorticity in the high-latitude ionosphere and its variation with interplanetary magnetic field direction and season. *Journal of Geophysical Research*, 114(A9), A09301. <https://doi.org/10.1029/2009JA014263>

Acknowledgments

GC was supported by the UK Natural Environment Research Council (NERC) highlight topic Grant NE/W003066/1 (FINESSE). He was also funded as part of the British Antarctic Survey (BAS) Polar Science for a Sustainable Planet Programme, funded by NERC. AGB and KAZ are supported by the Office of Naval Research. The authors would like to thank the NASA Space Physics Data Facility and National Space Science Data Center. The IMAGE FUV data were provided courtesy of the instrument PI Stephen Mende (University of California, Berkeley). We thank the PI, the IMAGE mission, and the IMAGE FUV team for data usage and processing tools. We thank Tom Sotirelis (Johns Hopkins University, Applied Physics Laboratory) for providing the DMSP boundary data base. The authors acknowledge the use of SuperDARN data. SuperDARN is a collection of radars funded by the national scientific funding agencies of Australia, Canada, China, France, Italy, Japan, Norway, South Africa, UK, and United States. The authors would like to thank the SuperDARN PIs of the radars which provided the original data for the vorticity data products: Glenn Hussey (University of Saskatchewan, Canada); J. Michael Ruohoniemi (Virginia Tech, USA); William Bristow (Penn State University, USA).

- Chisham, G., Lester, M., Milan, S. E., Freeman, M. P., Bristow, W. A., Grocott, A., et al. (2007). A decade of the Super Dual Auroral Radar Network (SuperDARN): Scientific achievements, new techniques and future directions. *Surveys in Geophysics*, 28(1), 33–109. <https://doi.org/10.1007/s10712-007-9017-8>
- Cowley, S. W. H., & Lockwood, M. (1992). Excitation and decay of solar-wind driven flows in the magnetosphere-ionosphere system. *Annales Geophysicae*, 10(1–2), 103–115.
- Davis, T. N. (1978). Observed characteristics of auroral forms. *Space Science Reviews*, 22(1), 77–113. <https://doi.org/10.1007/bf00215814>
- Dungey, J. W. (1961). Interplanetary magnetic field and the auroral zones. *Physical Review Letters*, 6(2), 47–48. <https://doi.org/10.1103/physrevlett.6.47>
- Eriksen, N. K., Lorentzen, D. A., Oksavik, K., Baddeley, L., Hosokawa, K., Shiokawa, K., et al. (2023). On the creation, depletion, and end of life of polar cap patches. *Journal of Geophysical Research*, 128(A12), e2023JA031739. <https://doi.org/10.1029/2023JA031739>
- Foster, J. C., & Burke, W. J. (2002). SAPS: A new categorization for sub-auroral electric fields. *Eos, Transactions American Geophysical Union*, 83(36), 393–394. <https://doi.org/10.1029/2002EO000289>
- Greenwald, R. A., Baker, K. B., Dudeney, J. R., Pinnock, M., Jones, T. B., Thomas, E. C., et al. (1995). DARN/SuperDARN: A global view of the dynamics of high-latitude convection. *Space Science Reviews*, 71(1–4), 761–796. <https://doi.org/10.1007/BF00751350>
- Hanuisse, C., Senior, C., Cerisier, J.-C., Villain, J.-P., Greenwald, R. A., Ruohoniemi, J. M., & Baker, K. B. (1993). Instantaneous mapping of high-latitude convection with coherent HF radars. *Journal of Geophysical Research*, 98(A10), 17387–17400. <https://doi.org/10.1029/93JA00813>
- Iijima, T., & Potemra, T. A. (1976). The amplitude distribution of field-aligned currents at northern high latitudes observed by Triad. *Journal of Geophysical Research*, 81(13), 2165–2174. <https://doi.org/10.1029/JA081i013p02165>
- Karlsson, T., Andersson, L., Gillies, D. M., Lynch, K., Marghitu, O., Partamies, N., et al. (2020). Quiet, discrete auroral arcs—Observations. *Space Science Reviews*, 216(1), 16. <https://doi.org/10.1007/s11214-020-0641-7>
- Kataoka, R., Chaston, C. C., Knudsen, D., Lynch, K. A., Lysak, R. L., Song, Y., et al. (2021). Small-scale dynamic aurora. *Space Science Reviews*, 217(17), 17. <https://doi.org/10.1007/s11214-021-00796-w>
- Landry, R. G., & Anderson, P. C. (2018). An auroral boundary-oriented model of subauroral polarization streams (SAPS). *Journal of Geophysical Research*, 123(A4), 3154–3169. <https://doi.org/10.1002/2017JA024921>
- Longden, N., Chisham, G., Freeman, M. P., Abel, G. A., & Sotiirelis, T. (2010). Estimating the location of the open-closed magnetic field line boundary from auroral images. *Annales Geophysicae*, 28(9), 1659–1678. <https://doi.org/10.5194/angeo-28-1659-2010>
- Lyons, L. R., Nishimura, Y., Zhang, S.-R., Coster, A. J., Bhatt, A., Kendall, E., & Deng, Y. (2019). Identification of auroral zone activity driving large-scale traveling ionospheric disturbances. *Journal of Geophysical Research*, 124(1), 700–714. <https://doi.org/10.1029/2018JA025980>
- MacDonald, E. A., Donovan, E., Nishimura, Y., Case, N. A., Gillies, D. M., Gallardo-Lacourt, B., et al. (2018). New science in plain sight: Citizen scientists lead to the discovery of optical structure in the upper atmosphere. *Science Advances*, 4(3), eaaq0030. <https://doi.org/10.1126/sciadv.aaq0030>
- Mende, S. B., Heeterdks, H., Frey, H. U., Lampton, M., Geller, S. P., Abiad, R., et al. (2000a). Far ultraviolet imaging from the IMAGE spacecraft. 2. Wideband FUV imaging. *Space Science Reviews*, 91(1–2), 271–285. <https://doi.org/10.1023/A:1005227915363>
- Mende, S. B., Heeterdks, H., Frey, H. U., Lampton, M., Geller, S. P., Habraken, S., et al. (2000b). Far ultraviolet imaging from the IMAGE spacecraft. 1. System design. *Space Science Reviews*, 91(1–2), 243–270. <https://doi.org/10.1023/A:1005271728567>
- Mende, S. B., Heeterdks, H., Frey, H. U., Stock, J. M., Lampton, M., Geller, S. P., & Lauche, H. (2000c). Far ultraviolet imaging from the IMAGE spacecraft. 3. Spectral imaging of Lyman- α and OI 135.6 nm. *Space Science Reviews*, 91(1–2), 287–381. <https://doi.org/10.1023/A:1005292301251>
- Newell, P. T., Burke, W. J., Sanchez, E. R., Meng, C.-I., Greenspan, M. E., & Clauer, C. R. (1991). The low-latitude boundary layer and the boundary plasma sheet at low altitude: Prenoon precipitation regions and convection reversal boundaries. *Journal of Geophysical Research*, 96(A12), 21013–21023. <https://doi.org/10.1029/91JA01818>
- Newell, P. T., Feldstein, Y. I., Galperin, Y. I., & Meng, C.-I. (1996). Morphology of nightside precipitation. *Journal of Geophysical Research*, 101(A5), 10737–10748. <https://doi.org/10.1029/95JA03516>
- Newell, P. T., Liou, K., Zhang, Y., Sotiirelis, T., Paxton, L. J., & Mitchell, E. J. (2014). OVATION Prime-2013: Extension of auroral precipitation model to higher disturbance levels. *Space Weather*, 12(6), 368–379. <https://doi.org/10.1002/2014SW001056>
- Nishitani, N., Ruohoniemi, J. M., Lester, M., Baker, J. B. H., Koustov, A. V., Shepherd, S. G., et al. (2019). Review of the accomplishments of mid-latitude Super Dual Auroral Radar Network (SuperDARN) HF radars. *Progress in Earth and Planetary Science*, 6(1), 27. <https://doi.org/10.1186/s40645-019-0270-5>
- Redmon, R. J., Peterson, W. K., Andersson, L., Kihn, E. A., Denig, W. F., Hairston, M., & Coley, R. (2010). Vertical thermal O⁺ flows at 850 km in dynamic auroral boundary coordinates. *Journal of Geophysical Research*, 115(A11), A00J08. <https://doi.org/10.1029/2010JA015589>
- Reidy, J. A., Fear, R. C., Whiter, D. K., Lanchester, B., Kavanagh, A. J., Milan, S. E., et al. (2018). Interhemispheric survey of polar cap aurora. *Journal of Geophysical Research*, 123(A9), 7283–7306. <https://doi.org/10.1029/2017JA025153>
- Reistad, J. P., Laundal, K. M., Østgaard, N., Ohma, A., Burrell, A. G., Hatch, S. M., et al. (2021). Quantifying the lobe reconnection rate during dominant IMF By periods and different dipole tilt orientations. *Journal of Geophysical Research*, 126(A11), e2021JA029742. <https://doi.org/10.1029/2021JA029742>
- Shepherd, S. G. (2014). Altitude-adjusted corrected geomagnetic coordinates: Definition and functional approximations. *Journal of Geophysical Research*, 119(A9), 7501–7521. <https://doi.org/10.1002/2014JA020264>
- Sotiirelis, T., & Newell, P. T. (2000). Boundary-oriented electron precipitation model. *Journal of Geophysical Research*, 105(A8), 18655–18673. <https://doi.org/10.1029/1999JA000269>
- Wu, C., Ridley, A. J., DeJong, A. D., & Paxton, L. J. (2021). FTA: A feature tracking empirical model of auroral precipitation. *Space Weather*, 19(5), e2020SW002629. <https://doi.org/10.1029/2020SW002629>
- Zhu, Q., Deng, Y., Richmond, A., McGranaghan, R. M., & Maute, A. (2019). Impacts of multiscale FACs on the ionosphere-thermosphere system: GITM simulation. *Journal of Geophysical Research*, 124(5), 3532–3542. <https://doi.org/10.1029/2018JA026082>